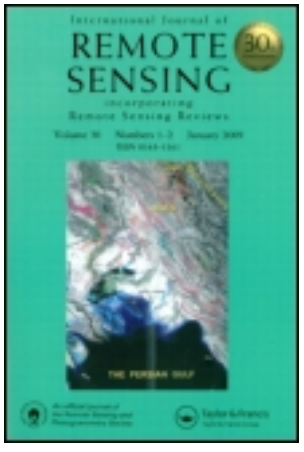

International Journal of Remote Sensing

Publication details, including instructions for authors and subscription information:
http://www.tandfonline.com/loi/tres20

Evaluating multiple colour-producing agents in Case II waters from Lake Erie

Joseph D. Ortiz[a], Donna L. Witter[a], Khalid Adem Ali[ab], Nathan Fela[a], Michael Duff[a] & Lonnie Mills[a]

[a] Department of Geology, Kent State University, Kent, OH 44242, USA

[b] Department of Geology and Environmental Geosciences, College of Charleston, Charleston, SC 29424, USA

To cite this article: Joseph D. Ortiz, Donna L. Witter, Khalid Adem Ali, Nathan Fela, Michael Duff & Lonnie Mills (2013) Evaluating multiple colour-producing agents in Case II waters from Lake Erie, International Journal of Remote Sensing, 34:24, 8854-8880

To link to this article: http://dx.doi.org/10.1080/01431161.2013.853892

International Journal of Remote Sensing, 2013
Vol. 34, No. 24, 8854–8880, http://dx.doi.org/10.1080/01431161.2013.853892

Taylor & Francis
Taylor & Francis Group

Evaluating multiple colour-producing agents in Case II waters from Lake Erie

Joseph D. Ortiz[a]*, Donna L. Witter[a], Khalid Adem Ali[a,b], Nathan Fela[a], Michael Duff[a], and Lonnie Mills[a]

[a]*Department of Geology, Kent State University, Kent, OH 44242, USA;* [b]*Department of Geology and Environmental Geosciences, College of Charleston, Charleston, SC 29424, USA*

(*Received 30 June 2011; accepted 8 July 2013*)

Lake Erie is part of the Great Lakes systems in North America, which represent the largest continental lake systems in the world. Anthropogenic eutrophication in the Western Basin of Lake Erie, a Case II environment, has an adverse impact on the surrounding ecosystems and the regional economy. The optical complexity found in Lake Erie is a feature of many aquatic environments making it a challenging setting for remote-sensing applications. To assess the controls on these optical properties, we sampled 20 locations, encompassing a variety of optical environments in the Western Basin and Sandusky Bay during four research cruises. Strong correlations between light extinction and phycocyanin (correlation coefficient, $r \geq 0.95$), suspended sediment ($r = 0.90$), and chlorophyll-*a* ($r \geq 0.86$) indicate that surface conditions are representative down to at least the first optical depth. Application of varimax-rotated principal component analysis to lab-based, hyperspectral reflectance data identified three components related to a diatom/green algae community, and two blue-green algae communities, one of which was associated with suspended sediment. Phycocyanin and chlorophyll-*a* content inferred using a semi-analytic red/near-infrared algorithm correlated well with concentrations measured *in situ* using a multiparameter sonde. Chlorophyll-*a* retrievals from a regional, blue : green algorithm developed for the Western Basin of Lake Erie compared well with retrievals from the semi-analytic algorithm for all samples from the Western Basin and 25% of samples from Sandusky Bay. Chlorophyll-*a* retrieval errors using the blue : green algorithm occurred when high ratios of suspended sediment to phycocyanin biased samples from the extremely turbid waters of Sandusky Bay. The bias likely resulted when suspended sediment altered the blue : green ratio or when phycocyanin interfered with the chlorophyll-*a* absorption peaks. This approach can be applied to other Case II environments to provide insights during the design of experimental field studies and for spectral band selection with the next generation of visible near-infrared remote-sensing instruments.

1. Introduction

Estimation of plant biomass in aquatic systems by retrieval of chlorophyll-*a* from remote-sensing observations has become routine in Case I waters, where chlorophyll-*a* is the dominant colour-producing agent (CPA) (McClain 2009). The situation is more complex in Case II waters, where multiple CPAs may confound the reflectance signal (Morel and Prieur 1977; Mobley et al. 2004). Bodies of water classified as Case II include coastal waters with significant input of suspended sediment and terrestrial organic matter, and shallow, highly stratified systems containing or dominated by blue-green algae or other

*Corresponding author. Email: jortiz@kent.edu

algal taxa with accessory pigments that alter the ratio of water-leaving radiances to each other, which vary *versus* wavelength. Many highly productive systems also have high concentrations of chromophoric dissolved organic matter (CDOM), degradation products of chlorophyll-*a*. In the Great Lakes Region, the Western Basin of Lake Erie is an excellent site to study the dynamics of Case II waters due to the input of several CPAs and the large range of observable conditions. Here, we seek to evaluate the relative importance of particulate CPAs in the Western Basin of Lake Erie and Sandusky Bay.

The Western Basin (WB) of Lake Erie and its generally more turbid marginal basin, Sandusky Bay (SB), exhibit these complicating factors. Productivity is among the highest seen in freshwater ecosystems, the maximum depth of the WB is only 11 m, and rivers draining eight major watersheds deliver a mix of sediment, CDOM, and riverine algae to the region. In addition to historical issues with Lake Erie water quality, in recent years the WB has experienced increasing blooms of *Microcystis aeruginosa*, a potentially toxic blue-green alga (Ouellette, Handy, and Wilhelm 2006; Millie et al. 2009). Efficient monitoring of water quality is essential because the lake serves as an economic and social resource through the fishing and recreation industries and is integral to the regional drinking water supply. While methods are being developed to monitor potentially harmful algal blooms in marine and coastal environments (Roesler and Boss 2008), these approaches are also necessary in aquatic environments.

While direct methods of monitoring water quality involve the analysis of water samples, these methods cannot provide the spatial and temporal coverage needed to continuously assess water quality on basin-wide scales. Use of satellite remote sensing provides complementary information with the potential to greatly improve our understanding of water quality variations (Baban 1995; Gons 1999; Nellis, Harrington, and Wu 1998; Islam, Yamaguchi, and Ogawa 2001; DeCauwer et al. 2004; Ouillon, Douillet, and Andrefouet 2004; Shuchman et al. 2006; Le et al. 2009; Park, Ruddick, and Lacroix 2010; Tarrant and Neuer 2009; Tyler et al. 2006). Remote-sensing systems assess water quality by applying algorithms that relate satellite-measured reflectance to the concentrations of specific CPAs (see Martin 2004). Ground-truthing is often achieved by comparing co-located satellite and *in situ* observations. Applying this technology to the WB of Lake Erie has proved challenging due to the difficulty of separating the spectral signatures of the multiple CPAs in the environment.

Recent work has demonstrated the difficulty of extracting valid chlorophyll-*a* information from the WB. Witter et al. (2009) evaluated retrievals of chlorophyll-*a* concentrations for Lake Erie employing 13 marine algorithms. They found that all of the ocean-calibrated algorithms had major deficiencies, and that the deficiencies were particularly large in the WB. Because the chlorophyll-*a* concentrations observed *in situ* in SB exceeded the maximum values for which the ocean-derived algorithms were calibrated, that region was excluded from their analysis. They also employed four regional algorithms specifically calibrated for Lake Erie that provided adequate performance in the Central and Eastern Basin, but which yielded relatively unsatisfactory results in the WB. Given the small size of the data set employed, additional observations were deemed necessary to fully validate the regional algorithms. Becker et al. (2009) employed a forward modelling method using a linear, non-negative, least-squares, spectral mixing model to infer phytoplankton abundance by class, and chlorophyll-*a* and phycocyanin concentrations in Lake Erie from Moderate Resolution Imaging Spectroradiometer (MODIS) observations. Their model produced results with generally good agreement when compared to *in situ* measurements (coefficient of determination, $R^2 = 0.66$ for cyanobacterial abundance), but they noted that additional work was needed to quantify

temporal variability in the characteristics of the CPAs. Wynne et al. (2010) monitored the dynamics of a *Microcystis* bloom in Lake Erie employing a Medium Resolution Imaging Spectrometer (MERIS)-based, spectral shape function (equivalent to a second derivative transformation), calibrated using cell counts obtained from filtered samples. Their work indicated that wind stress plays a major role in the distribution and intensity of algal bloom in surface waters, and therefore, wind data should be considered when evaluating the potential for prolonged bloom conditions.

Researchers working in other inland basins have had similar experiences. Randolph et al. (2008) employed an Analytical Spectral Devices (ASD; Analytical Devices, Inc., Boulder, CO, USA) FieldSpec™ UV–VNIR spectroradiometer, similar to the instrument used in this study, to estimate chlorophyll-*a* and phycocyanin in two reservoirs in Illinois with Case II water. They were able to predict the concentration of phycocyanin well using the algorithm of Simis, Peters, and Gons (2005), while chlorophyll-*a* prediction was less reliable. Because of the complexity of Case II waters, approaches that employ semi-analytical algorithms (Le et al. 2009) or spectral unmixing methods (Alcântara et al. 2009; Moberg et al. 2002) seem more effective at isolating the sources of variance present.

Our work is motivated by these studies. To further improve remote-sensing algorithms that will enable successful retrieval of chlorophyll-*a*, and potentially other CPAs in the WB, we explore the spectral reflectance of suspended materials collected in the WB and SB. Our approach is to use a laboratory-based, hyperspectral visible and near-infrared (VNIR) spectrometer to characterize the CPAs extracted from the particulate load in the water column. This enables us to capture the spectral signatures of particulate CPAs present in the region without the complications of variations in illumination or atmospheric interference, which interfere with remote-sensing observations.

We employ varimax-rotated principal component analysis (V-PCA), an inverse method in which the structure of the data determines the results of the decomposition. PCA has been successfully employed previously in ocean colour remote sensing for atmospheric correction and to improve the quality of chlorophyll-*a* retrievals (Frouin et al. 2005, 2006; Gross-Colzy et al. 2007; Steinmetz, Deschamps, and Ramon 2008).

2. Methods

2.1. Field methods

Using a research vessel from Stone Laboratories (*R/V Gibraltar III* or the *R/V Erie Monitor*), we conducted four research cruises on 11 June 2007, 27 June 2007, 29 July 2007, and 14 August 2007, collecting samples and a suite of measurements from 20 locations around the WB and in SB (Figure 1). These dates were selected subject to ship time availability and enabled us to sample a range of environmental conditions prior to and following the development of thermal stratification, which is associated with the development of cyanobacterial blooms in the warm summer months. Thin, high clouds and variable atmospheric aerosol content precluded direct comparison with either MODIS or Landsat overpasses, which coincided with the cruise dates. Completion of each cruise track, which was designed to collect water samples from a variety of environments, required approximately 10 hours. Sample locations were stored as waypoints using the Wide Area Augmentation System (WAAS)-enabled, Raymarine™ model C120/w (Raymarine, Inc., Nashua, NH, USA) on the *R/V Gibraltar III* or the Raymarine™ model C80 marine navigation system on the *R/V Erie Monitor* with guaranteed accuracy of <5 m and typical accuracy of <3 m to verify re-occupation of the same site during each cruise.

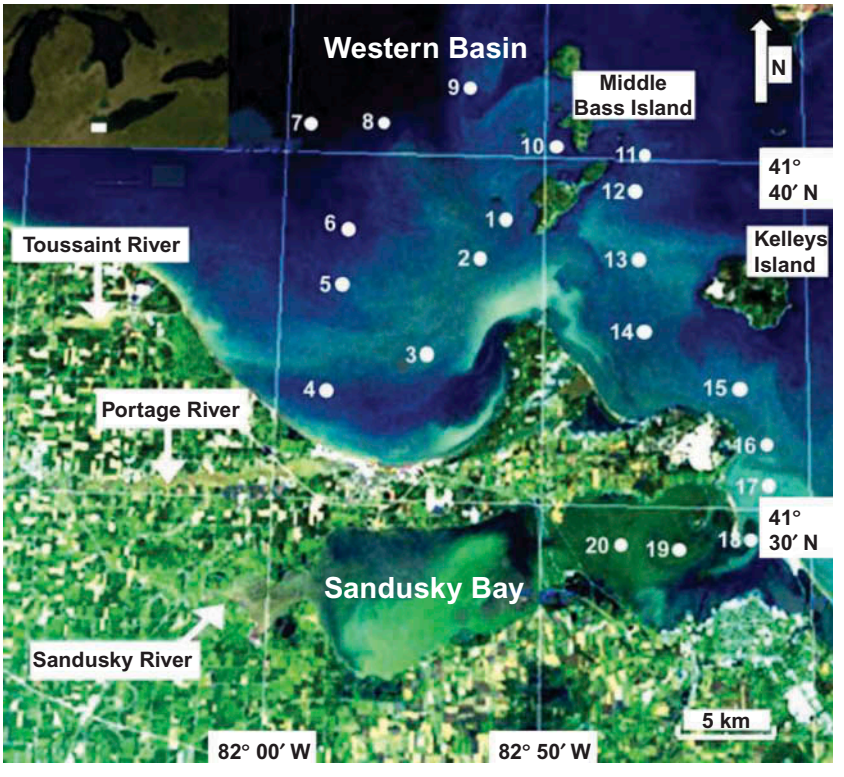

Figure 1. MERIS true colour image of the study area on 14 June 2007, indicating the positions of the 20 stations occupied during each of the four research cruises. Landmarks identified on the image include WB of Lake Erie, SB, and the major rivers (Sandusky, Toussaint, and Portage) feeding into these two bodies of water.

At each station, we measured Secchi depth and collected one litre of surface water for filtered reflectance measurement in the lab. Chlorophyll-*a* and phycocyanin concentrations were measured fluorometrically throughout the water column at each station using a depth-profiling, Hach Hydrolab DS5X multiparameter sonde (Hach Company, Loveland, CO, USA) fitted with two Turner Designs fluorometers (Turner Designs, Inc., Sunnyvale, CA, USA) that were factory calibrated prior to use. The instrument also measured depth, temperature, specific conductivity, pH, dissolved oxygen, oxidative–reductive potential, and turbidity in normalized turbidity units (NTUs). We compare the Hach Hydrolab surface values for selected parameters with filtered reflectance measurements from surface water collected at the same locations. The surface water was filtered onto a 47 mm glass-fibre filter (GF/F) during the cruise for later hyperspectral, VNIR derivative spectroscopy in the lab. All samples were wrapped in aluminium foil and stored on ice in the dark, until further processing, which took place the day following the research cruise. We evaluate the effectiveness of this method by correlating our lab results with field observations and by comparison with published reflectance spectra from high-performance liquid chromatography (HPLC)-extracted pigments (Toepel, Langner, and Wilhelm 2005). By filtering the samples, we concentrate the particulates extracted from the water column. This provides a sample analogous to a sediment sample, enabling us to apply methods that

have been effectively used to study the optical properties of lake sediment (e.g. Wolfe et al. 2006). This approach increases the signal to noise ratio but excludes CDOM from our measurements, which may be an important CPA in some of our samples. We thus provide insights into the particulate CPA signature in these water masses.

Secchi depths were measured on the shaded side of the vessel using a standard, 20 cm-diameter limnological Secchi disk with alternating black and white quadrants. The Secchi disk provides a measure that can be related to the light extinction coefficient (k_T). k_T itself is a composite optical property, $k_T = (\alpha + k_d)$, where α is the collimated light attenuation coefficient and k_d is the diffuse attenuation coefficient (Graham 1966; Tyler 1968; Lorenzen 1980; Armengol et al. 2003). This sum is also sometimes referred to as the 'light attenuation coefficient' (Kelble et al. 2005) and is proportional to the reciprocal of Secchi depth (m^{-1}) (Kelble et al. 2005). The Beers–Lambert law stipulates that k_T is proportional to increasing concentrations of CPAs, provided that the vertical light attenuation rate is constant. For Case II waters, the relationship can be written as

$$k_T = k_w + \alpha_{chl}C_{chl} + \alpha_{pcy}C_{pcy} + \alpha_{sed}C_{sed}, \quad (1)$$

where k_w is the diffuse attenuation due to pure water and k_d, the diffuse attenuation coefficient, has been partitioned into its constituent components, $\alpha_x C_x$, which represent the diffuse attenuation due to the concentrations of chlorophyll-*a* ($\alpha_{chl}C_{chl}$), phycocyanin ($\alpha_{pcy}C_{pcy}$), and suspended sediment ($\alpha_{sed}C_{sed}$), respectively. In Case I waters, this relationship simplifies because the terms $\alpha_{pcy}C_{pcy}$ for phycocyanin and $\alpha_{sed}C_{sed}$ for suspended sediment can be neglected.

2.2. *Laboratory methods*

In the lab, we determined the blank-corrected, dry particulate mass of each filter gravimetrically using an analytical balance with a precision of ±0.1 mg. The samples on the GF/F were dried overnight in an oven at 60°C, similar to the methods of Dabakk et al. (1999) and de Medeiros et al. (2005), who employed near-infrared (NIR) spectroscopy to study filtered seston in aquatic systems. Two hundred VNIR spectra were measured and averaged for each sample from the dried filters using an Analytical Spectral Devices (ASD) Labspec Pro FR ultraviolet/visible/near-infrared (UV/Vis/NIR) spectrometer equipped with a Labspec high-intensity contact probe. The system is capable of measuring reflectance between 250 and 2500 nm, at 2 nm resolution in the visible spectrum and 10 nm resolution in the NIR, on a 20 mm spot size. The data were then band-averaged to 10 nm width, providing hyperspectral resolution (210 bands) with useful observations between 400 and 2500 nm. The VNIR spectra were blank-corrected by dividing each sample reflectance spectrum by a GF/F blank reflectance spectrum measured in the same manner as the sample (e.g. Méléder et al. 2003; Combe et al. 2005). We report the results as percentage reflectance, because this is the measurement generated by our instrument. Recall that absorption, $a = \log_{10}(1/R)$, which can be approximated as $a = 1/R$ when the reflectance, R, is small. As such, a reflectance trough corresponds to an absorption peak. In applications where absorption is needed, we thus take the inverse of our reflectance measurements. The resulting percentage reflectance spectra were further transformed to produce two separate products: estimates of the concentrations of various CPAs calculated based on published remote-sensing algorithms and centre-weighted derivative spectra. The visible component of the derivative spectra was decomposed by V-PCA. The centre-

weighted first derivative of the reflectance spectra removes background scattering and accentuates absorption features in the visible and NIR spectra.

To evaluate the impact of filter drying on chlorophyll-*a* degradation, we searched the derivative of the measured reflectance spectra from our samples for features related to chlorophyll-*a* and its principle degradation products: phaeophytin-*a*, phaeophorbid-*a*, and chlorophyllide-*a*. We calculated derivative spectra from published HPLC-extracted reflectance spectra (Toepel, Langner, and Wilhelm 2005) from known pigments for comparison with our measurements. Our samples (see Figures 2 and 3) have peaks in their derivative

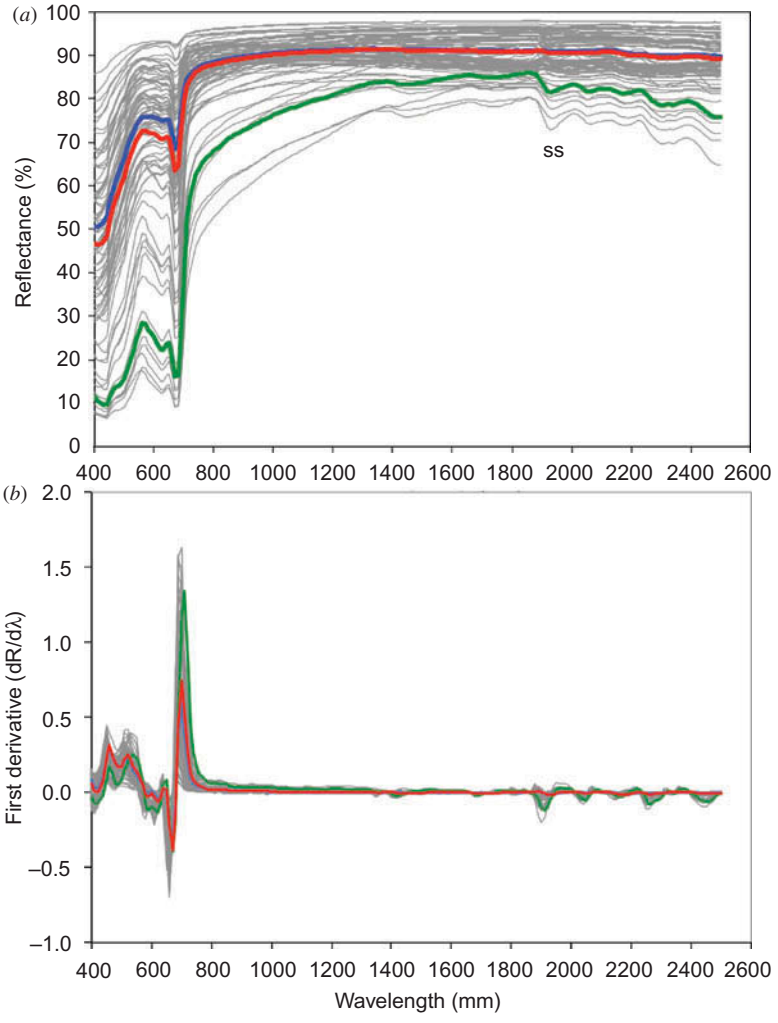

Figure 2. (*a*) Reflectance spectra (400–2500 nm) for all samples collected during the four research expeditions (grey curves). The blue curve is the average spectrum for the samples to the west of South and Middle Bass islands (Stations 1–10), while the red curve is the average spectrum for the samples east of South and Middle Bass islands (Stations 11–18) and the green curve is the average spectrum for the Sandusky Bay samples (Stations 19 and 20) from all cruises combined. The reflectance feature due to suspended sediment is denoted SS; (*b*) the centre-weighted first derivative of the reflectance spectra in Figure 2(*a*).

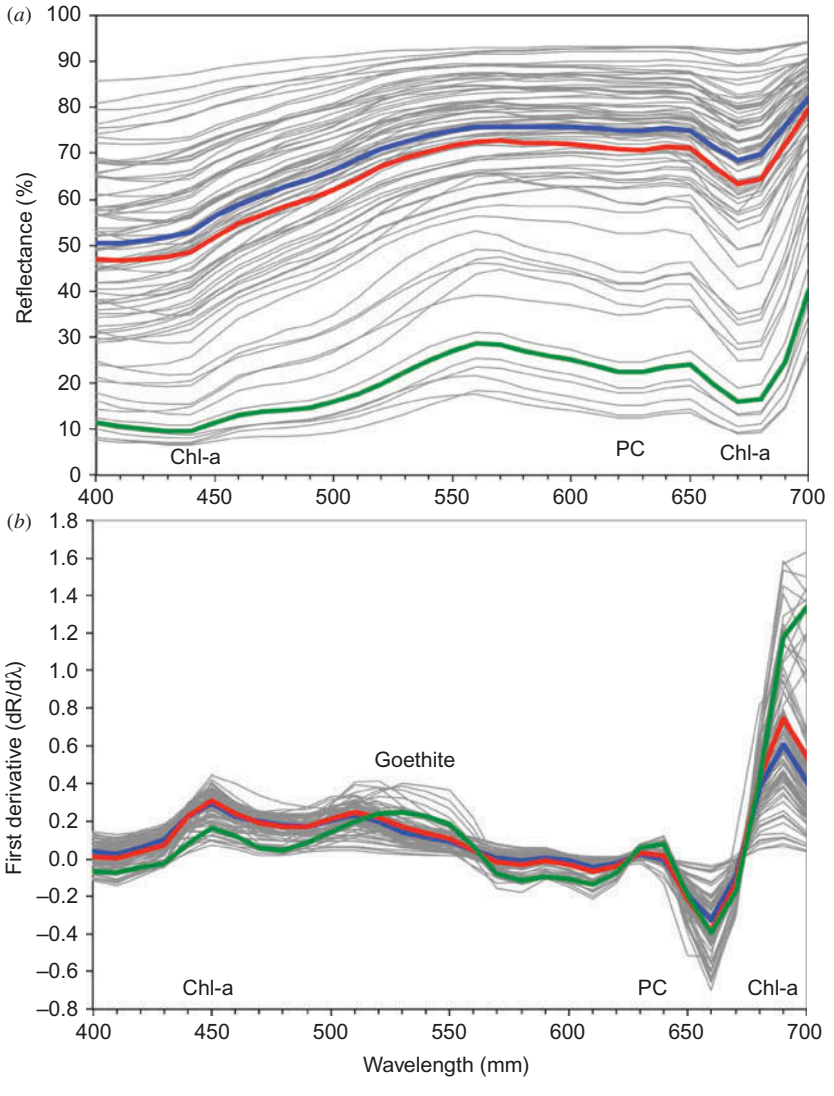

Figure 3. (*a*) The visible part of the reflectance spectra from Figure 4 identifying features associated with chlorophyll-*a* (chl-*a*) and phycocyanin (PC); (*b*) the centre-weighted first derivative of the visible part of the spectra. The grey, blue, red, and green curves are as defined in Figure 2. The suspended sediment feature in the visible spectrum can be identified as goethite based on its band position.

spectra at 450 nm and around 680–690 nm, similar to that observed for chlorophyll-*a* (450 and 670–680 nm). None of our samples exhibit derivative peaks at 420 nm, an indication of the presence of phaeophytin-*a* or phaeophorbid-*a* (Toepel, Langner, and Wilhelm 2005). Chlorophyllide-*a* has reflectance spectra similar to chlorophyll-*a* with derivative peaks at 440 and 680 nm. It can be differentiated from chlorophyll-*a* by its peak in the derivative spectra at 440 nm. However, we do not observe a peak at 440 nm in our samples, suggesting that either chlorophyllide-*a* is absent or its concentration is below a detectable level.

2.3. Quantification of CPAs

The complexity of Case II waters as described by Equation (1) requires that we monitor several classes of CPA to characterize the optical properties of the water. The bands of greatest interest include R_{490}, the reflectance at 490 nm, to monitor chlorophyll-*a* using the blue-green absorption region, R_{630}, the reflectance at 630 nm, to monitor phycocyanin, and R_{680}, the reflectance at 680 nm, to monitor chlorophyll-*a* in the red absorption region for chlorophyll-*a* (e.g. Simis, Peters, and Gons 2005; Witter et al. 2009; Yew-Hoong Gin et al. 2002; Wass et al. 1997; Alcântara et al. 2009).

We estimate variations in the relative concentration of various CPA by applying remote-sensing algorithms from the literature to our filtered, blank-corrected reflectance spectra. Although the results obtained from our filtered samples using these algorithms will likely be systematically offset from results using satellite data, we are most interested in the relative differences we observe between samples, rather than their absolute values. Our earlier work, Witter et al. (2009), provides motivation to focus on two classes of algorithms to estimate chlorophyll-*a*. We compare results depending on blue : green ratios and red : NIR ratios to evaluate the relative effectiveness of these band combinations for chlorophyll-*a* retrieval in the Case II waters of Lake Erie (e.g. Gitelson, Keydan, and Shiskin 1985; Gitelson 1992; Gitelson et al. 2008; Amin, Gilerson, et al. 2009; Amin, Zhou, et al. 2009; Gilerson et al. 2009). The results of this work should help to guide the selection of bands and band ratios on which to focus for the development of new remote-sensing algorithms and instrumentation to best retrieve pigment information for various classes of algae from remote-sensing data. Simis, Peters, and Gons (2005) provide semi-analytic algorithms to measure chlorophyll-*a* and phycocyanin corrected for biogenic backscatter (Gons 1999), water absorption (Buiteveld, Hakvoort, and Donze 1994), and the interference of the two pigments with each other. These algorithms are appropriate for our application because they were devised for use in shallow lakes dominated by blue-green algae. We also compared our results with a regional chlorophyll-*a* algorithm from Witter et al. (2009), which was derived based on co-located satellite observations and field-collected samples from the WB of Lake Erie. This algorithm is based on a comparison of remote-sensing reflectance for bands in the blue (490 nm) and green (555 nm) parts of the spectrum. In the Central and Eastern Basins, a similar regional algorithm, also calibrated with chlorophyll-*a* samples from Lake Erie, provides more effective chlorophyll-*a* retrievals than ocean-derived algorithms. Because the WB regional algorithm performed poorly in comparison with the Central and Eastern Basin regional algorithms from Witter et al. (2009), comparison of the WB regional algorithm with in-water data should help to diagnose the reasons for the algorithm's limitations.

To estimate suspended sediment (SS) concentration in our samples, we rely on a specific NIR band, 1910 nm, which should not be contaminated by the pigment signals in the visible. This measure of suspended sediment is based on the absolute value of the first derivative of the reflectance spectra, $\partial R/\partial\lambda$, where λ is wavelength:

$$\mathrm{ss} = \left|\frac{\partial R}{\partial \lambda}\right|_{1910}. \tag{2}$$

In the derivative of the reflectance spectra evaluated at 1910 nm, there is a prominent hydroxyl trough in siliciclastic minerals such as smectite or illite, two common clay minerals found in mid-latitude sediment (Clark et al. 2003; Viscara Rossel, McGlynn, and McBratney 2006; Jarrard and Vanden Berg 2006; Will 2006). Additional troughs at

greater wavelength in the NIR relate to carbonates present in our samples, as is expected given the regional bedrock geology. These troughs produce signals similar to the reflectance derivative feature at 1910 nm but yield a weaker signal. Because the reflectance derivative feature at 1910 nm is a trough in all samples, it generates a negative derivative in reflectance data. Calculating the absolute value provides a measure that increases linearly as suspended sediment concentration increases.

2.4. *Principal component analysis of reflectance spectra*

To complement the tests that we conducted with the remote-sensing algorithms, we also decomposed the blank-corrected, derivative-transformed, reflectance spectra to extract independent reflectance components, which can be compared to different classes of CPAs either independently or by calculating a contrast by subtracting one component from another. V-PCA (Kaiser 1958; Kachigan 1991; Smith 2002; Schlens 2005; Broersen, van Liere, and Heeren 2005) on the centre-weighted derivative of the reflectance spectra provides a powerful, multivariate approach to extract information regarding clay minerals, iron oxides/oxhydroxides, and plant pigments from visible spectra (Ortiz, O'Connell, and Mix 1999; Moberg et al. 2002; Ortiz et al. 2004, 2009). The strength of this inverse modelling method arises from its ability to determine linear combinations of the input variables that are orthogonal or independent, thus addressing the problem of correlated variance (multicollinearlity) inherent in most multivariate data sets, and effectively solving the potential problem of over-fitting to which forward, least-squares models are prone.

We conducted V-PCA on the correlation matrix obtained from a data matrix in which each column represents a 10 nm wavelength band of the derivative-transformed visible spectra, and each row represents a station in one of the cruise tracks. All four cruises were combined into a single matrix to allow evaluation of the joint variation in space and time within the data set. Use of the correlation matrix weights each band equally within the analysis because the correlation coefficient is the cross product of the z-scores of the two bands. We focused on the visible part of the spectrum because this is where the highest inter-correlations between bands are observed, facilitating extraction of V-PCA components.

Previous work has demonstrated the utility of this method for extracting information regarding variations in sediment composition (e.g. carbonates, clays, iron oxides, and oxyhydroxides) both spatially and temporally in bedrock, sediment, and suspended sediment aqueous mixtures (Balsam and Deaton 1991; Deaton and Balsam 1991; Mix, Harris, and Janecek 1995; Mix et al. 1999; Harris and Mix 1999; Lahet, Ouillon, and Forget 2000; Ouillon et al. 1997; Woźniak and Stramski 2004). The method works equally well with CPAs, allowing us to isolate spectral patterns that are correlated in space and time. To confirm that the results were not biased by outlier samples, we also performed versions of the V-PCA analysis on samples from the WB and SB separately.

3. Results

3.1. *CPAs inferred from filtered water samples*

The reflectance spectra for the 80 filtered, dried samples clearly showed evidence of multiple CPAs (Figure 2). The reflectance troughs at 450 and 680 nm correspond to chlorophyll-*a* absorption peaks, exhibiting values as low as 10%. For many samples,

particularly those in and near SB, a local minimum in absorption in the visible was observed between 560 and 580 nm, and phycocyanin absorption was observed between 620 and 630 nm with similarly low values (Figure 3). The minimum chlorophyll-*a* and phycocyanin absorption was observed at Stations 8 or 9 depending on the cruise. These two stations are located in relatively deep and open water, 4–10 km from land and 15–20 km from the nearest major river outflow. Based on visual inspection of Landsat images from previous years and MODIS/MERIS images from 2007 acquired within a 3 day window of our cruises, these sites are rarely influenced by riverine plumes. Analysis of additional MODIS/MERIS images from 2009 and 2010 is consistent with this observation. In Figure 2, the gradual increase in reflectance in the NIR is consistent with increasing suspended sediment concentration towards SB. Absorption in the NIR at 1400 nm, and 1910 nm and beyond, with values in the range of 60–70% for samples from SB, indicates the presence of suspended sediment (Clark et al. 2003; Viscara Rossel, McGlynn, and McBratney 2006).

3.2. *Spatial relationships of in-water properties and CPAs along cruise tracks*

Analysis of National Oceanic and Atmospheric Administration (NOAA) meteorological data from the South Bass Island Station, United States Geological Survey (USGS) stream flow data from the Maumee, Sandusky, and Portage Rivers, and hydrolab data collected during each cruise provide information on the environmental changes during the expeditions (Table 1, Figure 4). Atmospheric conditions during the cruises were similar: overcast skies with no rain and atmospheric pressure of 1017–1020 hPa and daily average southerly winds of 1.6 to 5 m s^{-1}, with the exception of the 29 June 2007 cruise when there was minor rainfall, and the 29 July 2007 cruise, during which the atmospheric pressure was 1014 hPa and the winds of 3.1 m s^{-1} were from the northeast. Air temperatures ranged from 20.7°C to 25.3°C. The warmest surface air temperatures occurred during the second cruise. Discharge from the Maumee, which was uncorrelated with that from the other rivers ranged from 11.33 to 30.6 m^3 s^{-1} during the span of the four cruises, while the discharge from the Sandusky (0.5 to 1.4 m^3 s^{-1}) and Portage Rivers (0.6 to 5.9 m^3 s^{-1}) was considerably lower, but inter-correlated. The average daily value for each variable fell within two standard deviations of its respective grand mean over the span of the four cruises.

The hydrolab data indicated that the surface temperatures – and stratification – increased during the course of the four cruises (Figure 5). On 11 June 2007, the surface temperature increased from 20.7°C at Station 1 to 24.8°C at Stations 19 and 20 (Figure 5). By the second cruise on 27 June 2007, the surface temperature at Station 1 had increased to 24.0°C while that at Station 20 had increased to 26.2°C. Temperatures at each station were similar or slightly cooler during the 29 July 2007 cruise relative to the 27 June 2007 cruise. By the fourth cruise, however, surface temperatures had increased considerably across the entire transect, with values of 25.8°C at Station 1, increasing only to 26.2°C at Station 20. Specific conductivity increased from Station 1 towards Station 20 in Sandusky Bay, but we observed no change in the average specific conductivity between cruises (Figure 5(*b*)).

The light extinction in the water column inferred from k_T generally increased from Station 1 (~0.5 m^{-1}) to Station 4 or 5 (~1.0 m^{-1}) depending on date (Figure 6(*a*)). Visual inspection of satellite imagery suggests that this trend coincides with the increasing influence of plumes associated with the Portage and Toussaint Rivers in the vicinity of these stations (see Figure 1). Light extinction generally decreased from Stations 4 to 10,

Table 1. NOAA South Bass Island Station daily averages of meteorological data and USGS stream gauge data.

Date DD-MM-YY	Wind Direction. (°)	Wind Speed (m s^{-1})	Gust Speed (m s^{-1})	Pressure. (hPa)	Atmospheric Temperature (°C)	Sandusky discharge (m^3 s^{-1})	Maumee discharge (m^3 s^{-1})	Portage discharge (m^3 s^{-1})
11 June 2007	200	1.6	1.9	1020	20.7	1.44	14.16	5.92
27 June 2007	188	5.0	5.7	1018	25.3	0.45	11.33	0.62
29 July 2007	46	3.1	4.7	1014	23.1	0.62	21.38	3.88
13 August 2007	178	3.4	4.6	1018	23.6	1.02	30.58	2.72
Average	153	3.3	4.2	1017	23.2	0.88	19.36	3.28
Standard deviation	72	1.4	1.6	3	1.9	0.44	8.59	2.21

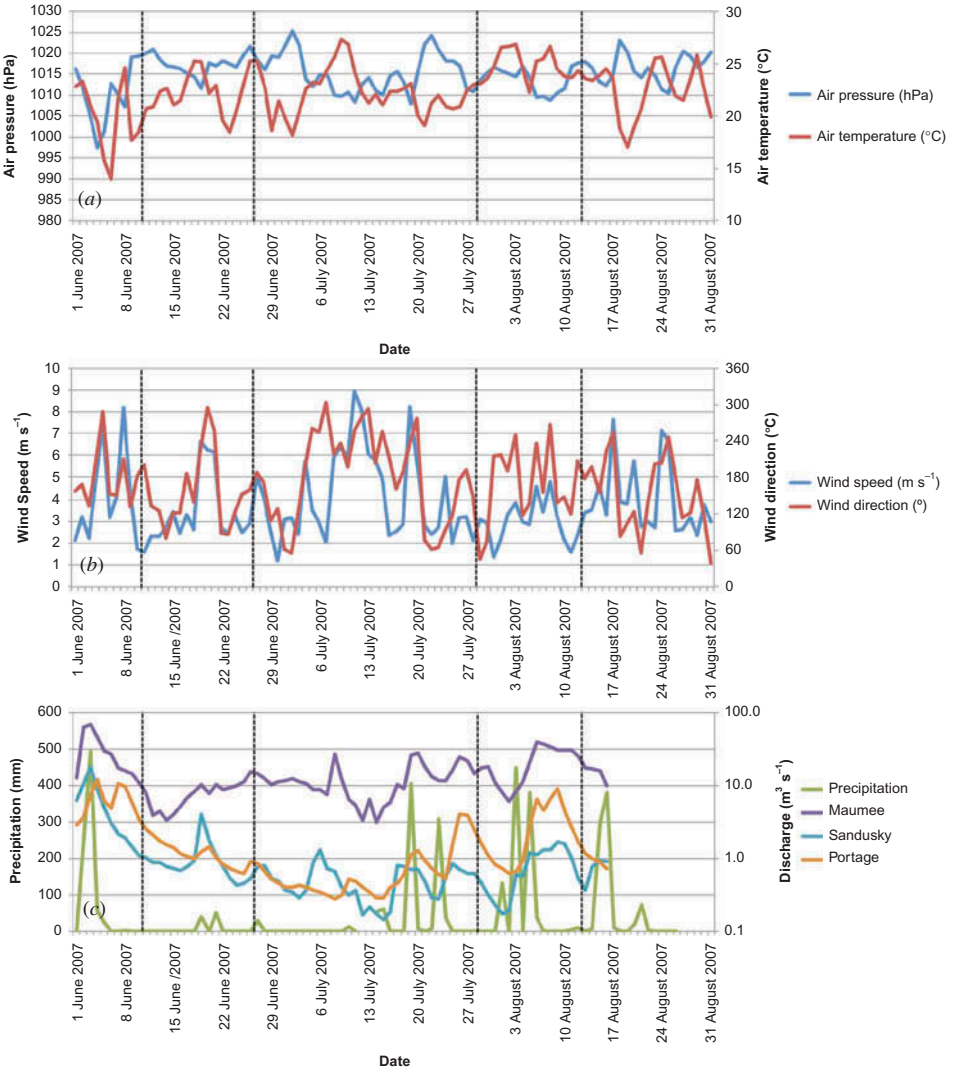

Figure 4. Daily averages of meteorological data spanning the cruise intervals for NOAA South Bass Island Station: (*a*) air pressure and air temperature; (*b*) wind speed and wind direction; and (*c*) precipitation and USGS stream gauges for Maumee R., Sandusky R., and Portage R.

reaching a minimum of ~0.25 m^{-1} between Stations 8 and 10, depending on the date of the cruise. The greatest increase in k_T was observed from Station 11 to Station 20, transiting from the Lake Erie Islands into SB. During all cruises, the stations in SB exhibited the highest values of k_T. The maximum value of k_T observed at Station 20 ranged from 2 to 3.25 m^{-1} and increased from the first to the fourth cruise. The concentration of filtered, dried, total suspended particulates (TSP) generally follows the trends in k_T (Figure 6(*a*)) with minimal values that were essentially zero to values as high as 40 mg l^{-1} at Station 20. Plant pigment and suspended sediment produce spatial and temporal patterns that are generally consistent with the k_T and TSP data obtained from the matching cruise track (Figure 6). Comparisons of pigment retrievals from the

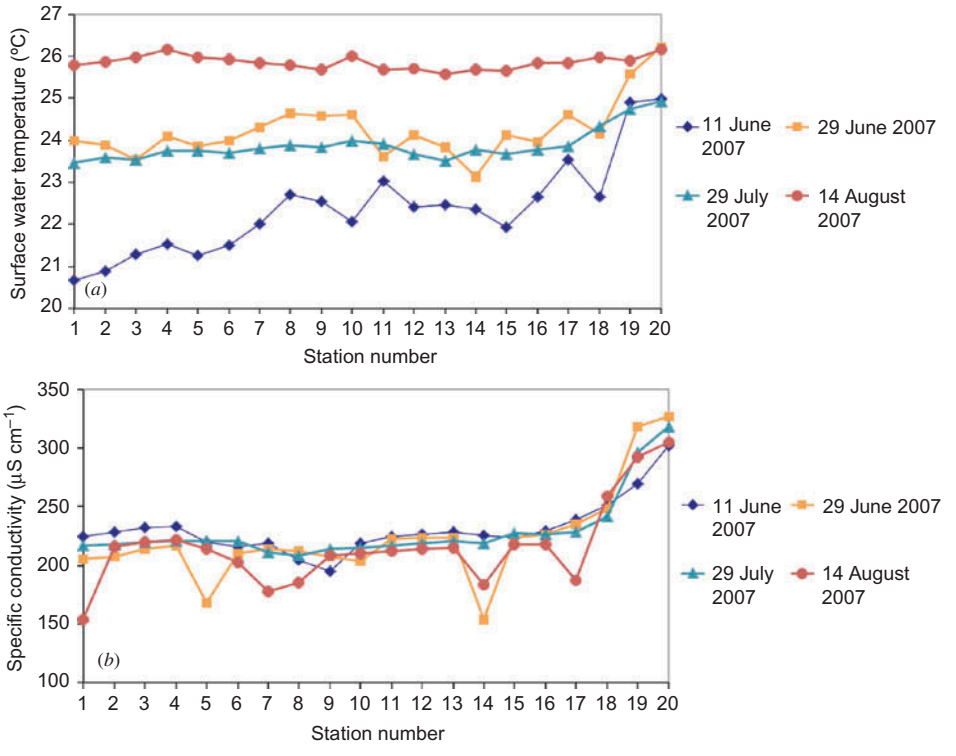

Figure 5. Surface water temperature (*a*) and specific conductivity (*b*) during the four cruise dates: 11 June 2002 (blue curve), 29 June 2007 (orange curve), 29 July 2007 (cyan curve), and 14 August 2007 (red curve).

remote-sensing algorithms of Simis, Peters, and Gons (2005) and the regional WB algorithm of Witter et al. (2009) show similar trends in the WB, with values generally below 2 µg l^{-1}. In SB, a region for which the Witter et al. (2009) algorithm employed did not include calibration data, it produced much higher mean chlorophyll-*a* values (10–18 µg l^{-1}) than the Simis, Peters, and Gons (2005) algorithm (3–4 µg l^{-1}), which is optimized for use in hyper-eutrophic environments. The trends in the relative measure of suspended sediment were similar to those displayed by the Witter et al. (2009) algorithm.

3.3. *Relationships between multiple measures of CPAs*

When considered for all 20 stations, most of the CPAs studied were highly correlated (correlation coefficient, $r \geq 0.86$) with k_T (Table 2), indicating that multiple CPAs control the optical environment of the region as a whole. The majority of correlation values were statistically significant (Table 2). Inspection of correlations calculated separately for the WB stations (1–18) and the SB stations (19–20) reveals that the optical regime differs between these two areas. In the WB, with the exception of the Hydrolab chlorophyll-*a* estimate, correlations between k_T and phycocyanin, chlorophyll-*a*, and suspended sediment were very strong ($r \geq 0.80$), indicating that variations in these CPAs control regional variations in absorption. Hydrolab phycocyanin estimates are well correlated with k_T in both the WB and SB. Although suspended sediment attains its highest values in SB

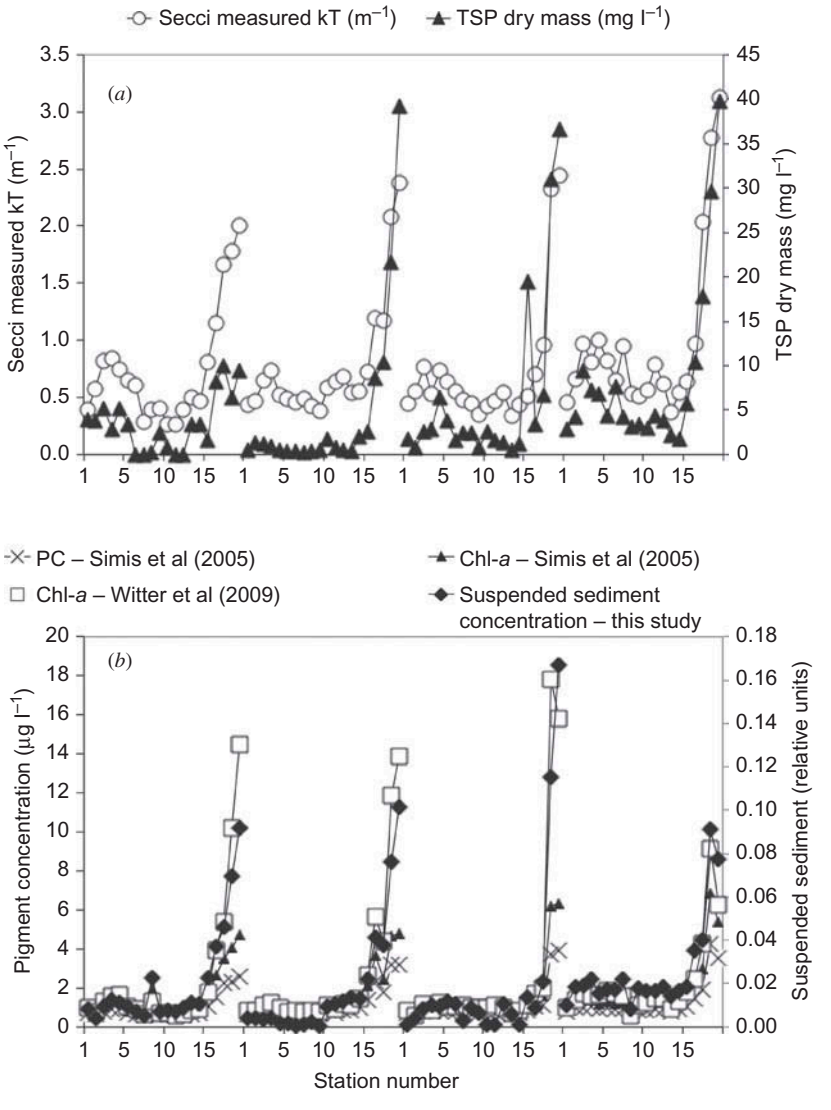

Figure 6. (*a*) Light extinction and total suspended particulate mass and (*b*) chlorophyll-*a*, phycocyanin (PC), and suspended sediment estimates for all samples collected during the research cruises. The sample locations are as defined in Figure 1 and the text. Sample 1 is located at Middle Bass Island, Sample 20 in SB. The data are presented in chronologic order with the earliest cruise on the left.

(Figure 6(*b*)), variations in this variable do not correlate significantly with variations in k_T within SB, where there are much stronger relationships between k_T and phycocyanin.

3.4. Principal component analysis of derivative-transformed reflectance spectra

The V-PCA model based on the entire data set extracted three significant varimax-rotated components, which account for 39.9%, 30.0%, and 22.3% of the variance for a combined

Table 2. Values of Pearson correlation coefficient (r*) for the correlation between total attenuation coefficient (k_T) and CPA measures.

Variable (CPA measure)	WB and SB Stations 1–20 (n = 80)	WB Stations 1–18 (n = 72)	SB Stations 19–20 (n = 8)
Phycocyanin (red : NIR) (Simis, Peters, and Gons 2005, their Equation (5))	0.95	0.84	0.73
Phycocyanin (Red : Red) (Hach Hydrolab)	0.91	0.87	0.97
Chlorophyll-*a* (red : NIR) (Simis, Peters, and Gons 2005, their Equation (3))	0.95	0.81	0.62†
Chlorophyll-*a* (blue : Red) (Hach Hydrolab)	0.59	0.57	0.90
Chlorophyll-*a* (blue : Green) (Witter et al. 2009)	0.86	0.85	–0.46†
Suspended Sediment (This study, Equation (2))	0.90	0.80	0.12†

Notes: *All correlations significant at $p < 0.01$ level unless otherwise marked. †Correlation not different from zero at the $p = 0.05$ level.

total variance explained of 92.2%. The average communality for the 30 bands was 0.92 out of 1.0, and so these three components contributed to the vast majority of spectral variability at each station. Comparison of the component loadings as a function of wavelength with derivative-transformed standard reflectance spectra for pigments from known classes of algae extracted by HPLC and sediment minerals indicates that the first component is inversely correlated with prokaryotic blue-green algae (Figure 7(*a*)). We plot this component on an inverted axis so that its sense of increase matches that of the other components. The second component relates to eukaryotic diatoms and/or green algae (Figure 7(*b*)). The third component represents a more complex mixture, blue-green algae, and the iron oxyhydroxide, goethite (Figure 7(*c*)). The reference spectrum in Figure 7(*c*) was obtained from a least-squares fit of the component-3 loadings to a linear mixture of blue-green algae and goethite derivative spectra.

Comparison of the component scores at each site allows us to evaluate the relative importance of each component along each cruise track (Figure 8(*a*)). For three of the four cruises, the first component has its strongest component scores in SB (−1.5 standardized units), suggesting that lacustrine blue-green algae concentrations were greatest in SB. In the WB, Component 1 scores were highest for cruise 2 (−0.5 to −1.0 standardized units), when daily-averaged air temperatures were 2°C to 4°C warmer than during any of the other cruises as measured at the National Oceanic and Atmospheric Administration's South Bass Island Station located near our Station 1. The warm temperatures on the day of cruise 2 and on the days immediately preceding this cruise may have generated conditions conducive to blue-green algae growth in the WB (Millie et al. 2009). Surface water temperatures at our stations during the second cruise also increased by up to 3°C from our first cruise, an indication of greater stratification of the lake during the summer. Component 2 scores, indicative of the diatom/green algae community, are generally lower in SB (−1 to −2 standardized units) than in the WB (1−2 standardized units), suggesting that this assemblage is more important in the WB than in SB. Component 3 decreases in importance with time in SB, from 4 to −1 standardized units, perhaps due to increasing stratification and/or decreasing nutrient availability.

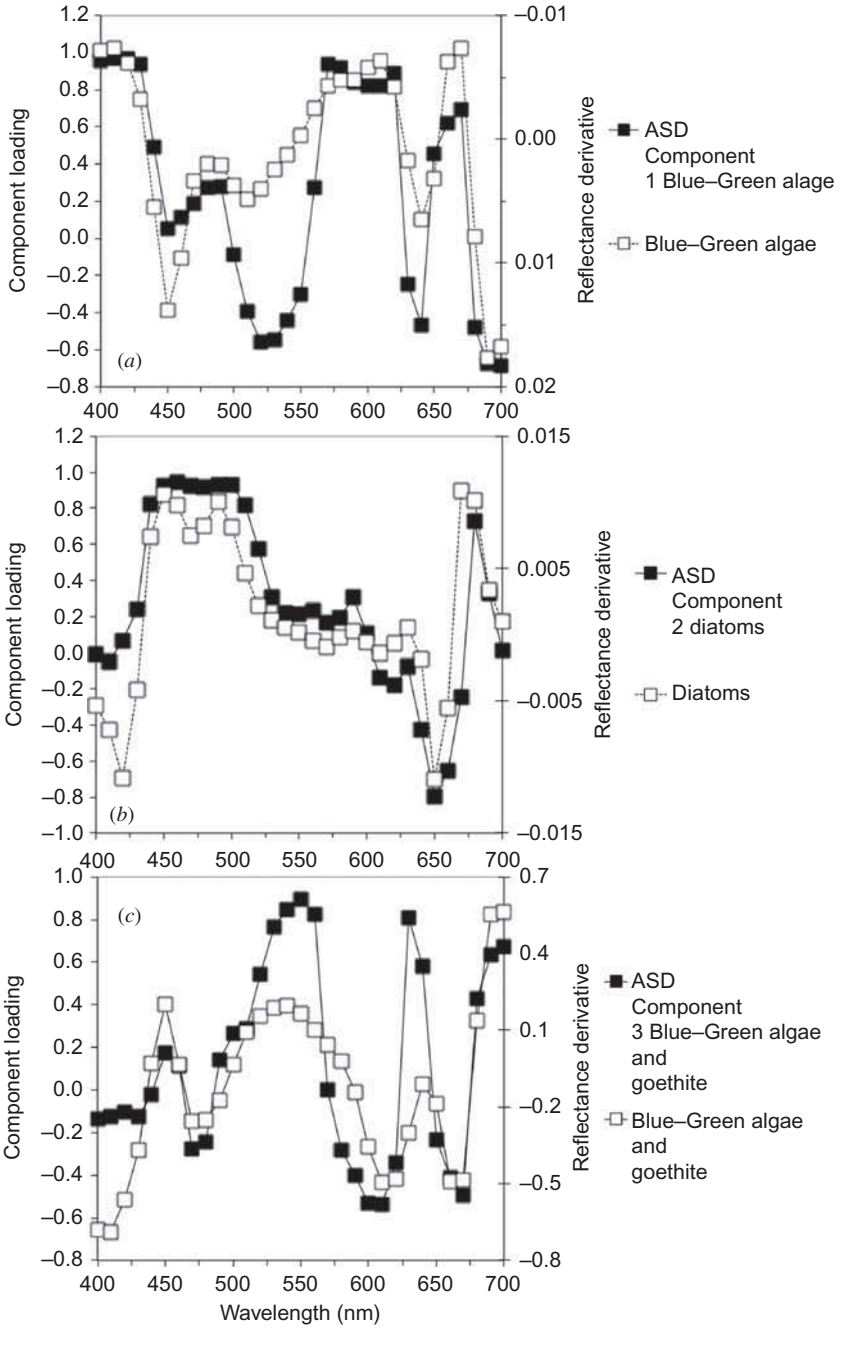

Figure 7. Component loadings for the V-PCA and selected reference spectra. (*a*) The first component relates to blue-green algae, (*b*) the second component relates to diatoms and green algae, and (*c*) the third component relates to a mixture of blue-green algae and goethite, an iron oxyhydroxide component of the suspended sediment.

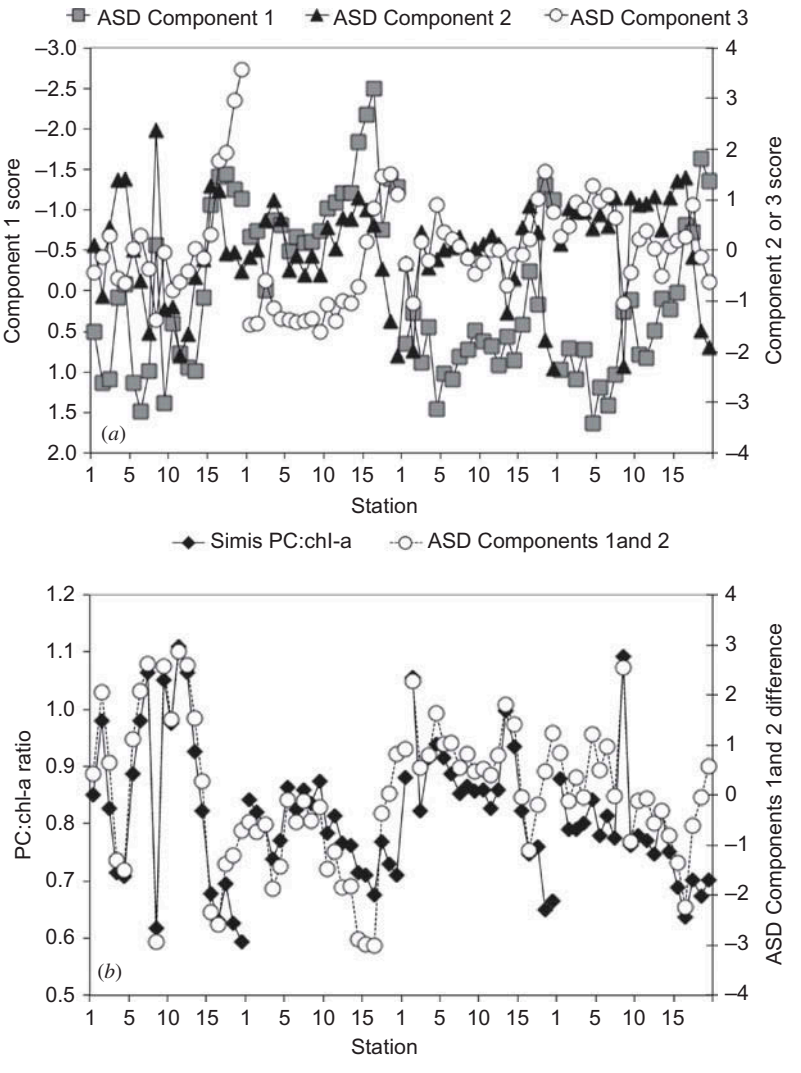

Figure 8. (*a*) Component scores from the V-PCA model *versus* station. The importance of each component in each sample is proportional to its magnitude; (*b*) the phycocyanin (PC) to chlorophyll-*a* ratio (PC : chl-*a*) is proportional to the difference between the first and second components, as described in the text. The sample locations are as defined in Figure 1 and the text.

The results from the component analysis are consistent with the variance in the Hydrolab chlorophyll-*a* and phycocyanin estimates. In SB, the correlations of k_T *versus* chlorophyll-*a* and suspended sediment based on several remote-sensing algorithms are generally lower than in the WB or the combined data set (Table 2), suggesting regional shifts in the relative proportions of plant pigments present in the SB and thus a regional change in the phytoplankton community structure within the SB relative to the WB. We can quantify this change in phytoplankton community structure by calculating the contrast between two components. This is done by subtracting the component scores of the second component from those of the first (i.e. Component 1−2 contrast = Component 1 minus

Component 2). This demonstrates a change in sign of the phycocyanin to chlorophyll-*a* (chl-*a*) ratio relative to the Component 1−2 contrast between samples from the WB and SB (Figure 8) The Component 1−2 contrast is positively correlated with the phycocyanin (PC)–chl-*a* ratio in the WB, but inversely correlated in SB.

To confirm that outliers from SB did not control our results, we re-computed the component analysis for data from WB only and SB only. The primary differences when SB was excluded were that the importance of Components 1 and 2 switched and the amplitude of the goethite peaks in Component 3 (at around 450 and 550 nm) either decreased or separated from the blue-green algae component of Component 3 as a fourth, distinct component. This confirms our interpretation of Component 3 in the V-PCA based on the entire data set as a different community of blue-green algae associated with suspended sediment in the SB. The prominent role played by suspended sediment – as represented by the iron oxyhydroxide goethite in this component – suggests that these blue-green algae may be of riverine origin or could be stimulated by mixing events, which stir sediment and iron oxyhydroxides from the bottom of the lake to its surface. These results also indicate that samples 16–18 represent intermediate mixtures of WB and SB assemblages as can be inferred from their geographic position.

4. Discussion

4.1. Impact of multiple CPAs on optical properties of Case II water in WB and SB

The strength of our approach arises from the use of multivariate statistical methods to partition the signatures of multiple CPAs through analysis of whole waveforms extracted numerically from the visible part of the reflectance derivative spectra. Prior studies have demonstrated the effectiveness of this type of approach using lab- and/or field-based hyperspectral derivative spectroscopy to study complex aquatic environments (Demetriades-Shah, Stevens, and Clark 1990; Han and Rundquist 1997; Méléder et al. 2003; Becker, Lusch, and Qi 2005; Combe et al. 2005; Barille et al. 2007; Murphy et al. 2008). Analysis of our data indicates that diffuse attenuation due to plant pigments and suspended sediment increases from the WB into SB, although the variability of this trend changes according to the component (Figure 8). We observed strong linear correlations between the CPAs and k_T at our sites (Table 2), demonstrating that surface conditions are representative of diffuse attenuation down to at least the first optical depth, from which the majority of the satellite response is received.

Chlorophyll-*a* estimates from the Witter et al. (2009) and Simis, Peters, and Gons (2005) algorithms matched well for samples from Stations 1–18 during all cruises and for samples from Stations 19–20 in SB collected during cruise 4 (Figure 9, Table 3), despite the fact that these algorithms are based on different bands and have different functional forms. However, estimates from the two algorithms diverged in SB for samples from Stations 19–20 collected during the first three cruises. For these samples, estimates from the Witter et al. (2009) algorithm were biased high (up to 8.9 μg l^{-1}) relative to results from the Simis, Peters, and Gons (2005) algorithm (Figure 9, Table 3). These biased samples correspond to samples with high concentrations of phycocyanin and suspended sediment.

Our sample distribution allows us to evaluate how the interaction of phycocyanin and suspended sediment influences the observed chlorophyll-*a* bias between the algorithms we studied. The phycocyanin estimates from the Hach Hydrolab sonde are reasonably well correlated with the phycocyanin estimates from the Simis, Peters, and Gons (2005)

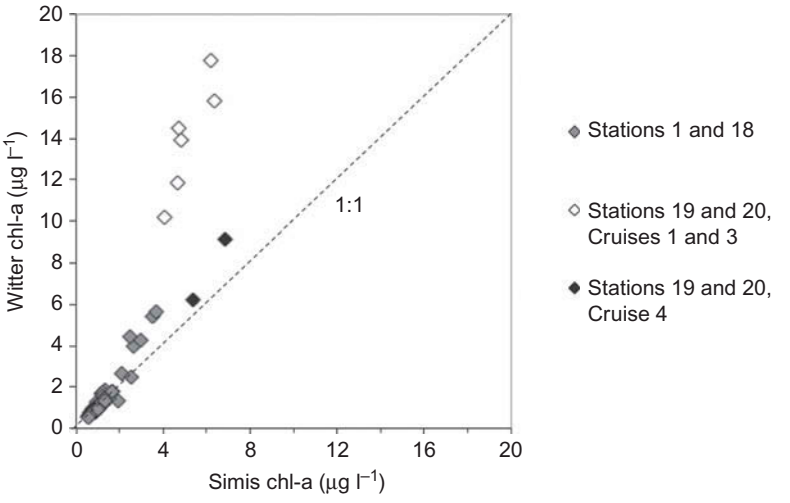

Figure 9. Comparison of the semi-analytic algorithm of Simis, Peters, and Gons (2005) with the Lake Erie regional algorithm of Witter et al. (2009) demonstrates that the two methods agree for samples from the WB, but diverge for most samples from SB.

Table 3. Statistical comparison of chlorophyll-*a* errors for the algorithm of Witter et al. (2009).

Proxy	Bias (µg l^{-1})	RMSE (µg l^{-1})
Stations 1–18, Cruises 1–3	0.2	0.4
Station 19–20, Cruise 4	1.6	1.0
Stations 19–20, Cruises 1–3	8.9	2.0

Notes: Blue : green algorithm relative to the Simis, Peters, and Gons (2005) red : NIR algorithm. RMSE is the root mean square error.

phycocyanin algorithm (Table 4). The Hach Hydrolab sonde observations for chlorophyll-*a* are also more strongly correlated with the Simis, Peters, and Gons (2005) than the Witter et al. (2009) chlorophyll-*a* retrievals in SB (Table 4). In remote-sensing applications in water, 'suspended sediment spectra' are often presented which exhibit maximum reflectance near 500–650 nm and greater absorption towards the blue and red ends of the spectrum (Wass et al. 1997; Alcântara et al. 2009). These features are not replicated in spectrophotometric observations of dried, filtered sediment (Clark et al. 2003; Montero Sanchez et al. 2001; Jarrard and Vanden Berg 2006), and thus this spectral shape likely results from the interaction of suspended sediment with the absorption of water and other CPAs in the water column (Bukata, Bruton, and Jerome 1983). Likewise, because the contribution of chlorophyll-*a* to R_{550} is minimal, this band is sometimes used to gauge the suspended sediment contribution in remote-sensing applications (Wass et al. 1997). However, in the WB samples from our data set, R_{550} is highly correlated with visible bands out to 700 nm, but uncorrelated with NIR bands with known sediment absorption features. While the chlorophyll-*a* contribution at 550 nm is minimal, phycocyanin exhibits its maximal absorption at 620–630 nm with a broad peak that extends down towards 550 nm at the blue-green end of the spectrum and towards 700 nm at the red end of the spectrum (Robertson, Lawton, and Cornish 1999). Peng et al. (2007) observed a strong

Table 4. Values of Pearson correlation coefficient (r*) for the correlation between Hach Hydrolab sonde and remote-sensing algorithm estimates.

Proxy	WB and SB Stations 1–20 (n = 80)	WB Stations 1–18 (n = 72)
Witter et al. (2009) Blue-Green chlorophyll-*a* algorithm *versus* Hydrolab chlorophyll-*a*	0.39	0.63
Simis, Peters, and Gons (2005) Red : NIR chlorophyll-*a* algorithm *versus* Hydrolab chlorophyll-*a*	0.60	0.71
Simis, Peters, and Gons (2005) Red : NIR phycocyanin algorithm *versus* Hydrolab phycocyanin	0.88	0.85

Note: *All correlations significant at $p < 0.01$ level.

linear relationship between particulate backscatter measured at 555 or 650 nm, denoted b_p (555) and b_p (650), respectively, for samples from a variety of aquatic environments in New York State. This is because variations in algal cell density result in scattering that influences reflectance in the range 550 to 700 nm (Schalles 2006). Beyond 700 nm, scattering effects in the NIR region are controlled by suspended sediment. As a final point, carotenoid pigment also contaminates R_{550} by eroding the left shoulder of the R_{550} peak (Schalles and Yacobi 2000). Due to these pigment- and cell-scattering influences, R_{550} cannot be used effectively as a measure of suspended sediment in the Case II waters of Lake Erie, and potentially in other Case II waters.

4.2. *Potential mechanisms of pigment bias in Case II water of Lake Erie*

To compare the properties that potentially influence the chlorophyll-*a* bias, we calculated the ratio of SS as described above to PC as measured by the Simis, Peters, and Gons (2005) phycocyanin algorithm (Figure 10). This ratio, which we denote SS/PC, indicates that the SB samples with the highest chlorophyll-*a* bias (values greater than 5 μg l^{-1}) also have high amounts of suspended sediment relative to the amount of phycocyanin (ratios greater than 1.25). The absorption response of suspended sediment results in bias for remote-sensing algorithms that compare band ratios across the visible spectrum. Samples from SB had higher levels of suspended sediment than samples from the WB (Figure 6(*b*)) contributing to the outliers identified in Figure 10. The most likely cause for the bias in chlorophyll-*a* estimation in these samples appears related to suspended sediment. Samples with SS/PC >1.25 resulted in biased chlorophyll-*a* retrievals using the blue : green band ratio algorithm (Figure 10). Samples with intermediate and low values of SS/PC (<1.25) resulted in relatively unbiased chlorophyll-*a* estimates when using the same algorithm. A plausible mechanism to explain the bias in the Witter et al. (2009) algorithm is that similar to other blue : green ratio algorithms, it is sensitive to the impact of suspended sediment as well as pigments on the green portion of the spectrum near 550 nm. In our particular environment, the presence of goethite, an iron oxyhydroxide in the suspended sediment, may also have posed a serious problem. The derivative spectrum from goethite exhibits the greatest rate of change at 545 nm, close to the 550 nm normalizing band employed in the Witter et al. (2009) algorithm. The Simis, Peters, and Gons (2005) semi-analytic

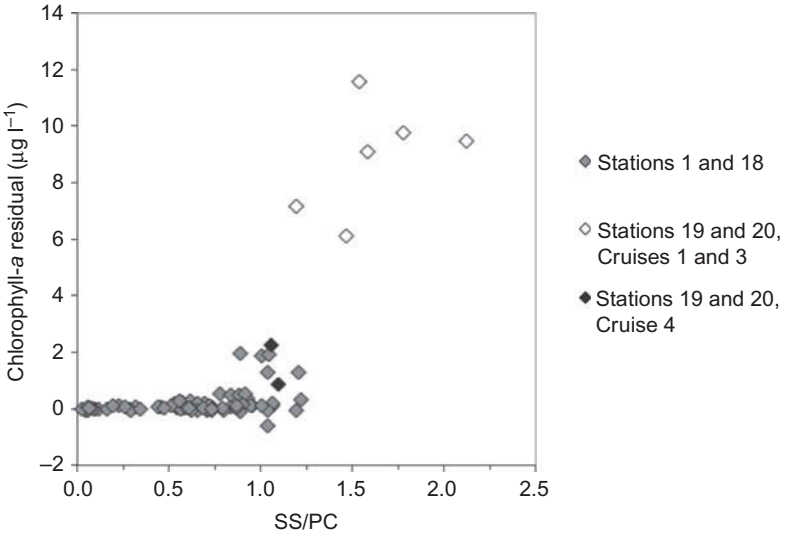

Figure 10. Relationship between the ratio of suspended sediment to phycocyanin (SS/PC) and the chlorophyll-a residual (µg l^{-1}) estimated as the difference between the Witter et al. (2009) algorithm and the best-fit line between the two algorithms − Witter et al. (2009) and Simis, Peters, and Gons (2005) − for samples from Sandusky Bay.

algorithm does not have this issue because it is a red : NIR ratio algorithm and thus avoids this potential source of bias.

For cases with low to intermediate suspended sediment concentrations (i.e. the WB and SB cruise 4 data), the chlorophyll-*a* bias increases with increasing phycocyanin concentration. Of these two effects on the chlorophyll-*a* bias, suspended sediment *versus* phycocyanin, the effect of suspended sediment appears to create the greatest problem for chlorophyll-*a* retrievals in these samples. In Lake Erie, it is important to note that the conditions that generate this suite of correlated errors are most common in the WB and SB, although events such as high fluvial discharge and sediment re-suspension could produce these conditions in other areas of the lake. As noted by Witter et al. (2009), the regionally tuned, blue : green algorithms performed much better in the Central and Eastern Basins of Lake Erie in deeper water and away from major fluvial input.

The interaction of chlorophyll-*a* and phycocyanin on the remote-sensing algorithms results in a more subtle form of bias. In cases where there is light to moderate loading of suspended sediment, or in blue-green algal blooms, the concentration of phycocyanin becomes a factor that affects the quality of the chlorophyll-*a* retrievals with algorithms that use blue : green ratios. To demonstrate this, we calculated weighted average reflectance spectra by numerically mixing a pure chlorophyll-*a* and a pure phycocyanin end member in different proportions (Figure 11). This simple model demonstrates the impact of phycocyanin reflectance on chlorophyll-*a* reflectance and *vice versa*. Chlorophyll-*a* and phycocyanin peak in different parts of the electromagnetic spectrum. Indeed, accessory pigments such as phycocyanin evolved to capitalize on this difference (Sze 1986). There is, however, overlap between the responses of these two pigments (Figure 11(*a*)), which biases remote-sensing chlorophyll-*a* algorithms based on blue–green bands in two important ways. Because phycocyanin is highly reflective towards the blue end of the spectrum, it increasingly masks the chlorophyll-*a* absorption peak at 440 nm as its relative

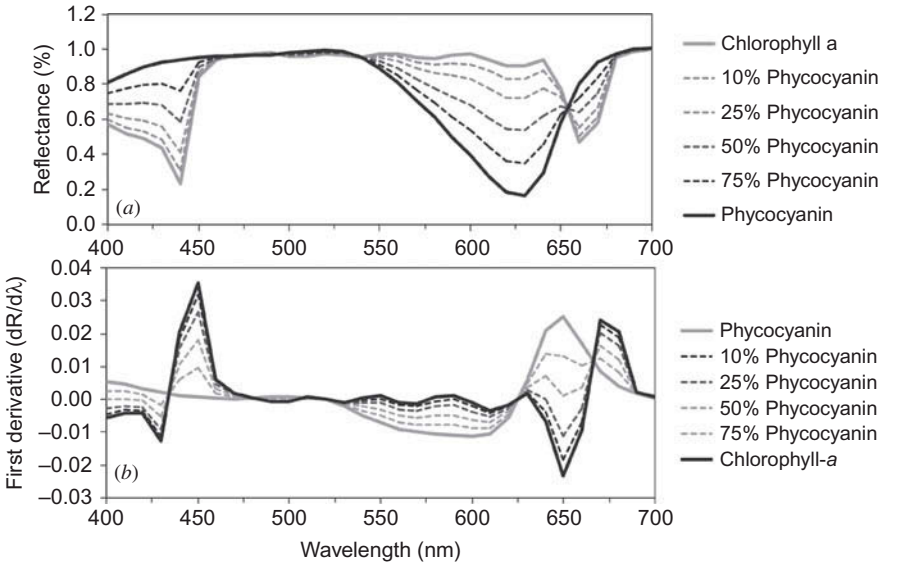

Figure 11. Reflectance (*a*) and first derivative (*b*) spectra generated using a linear mixing model for chlorophyll-*a* and phycocyanin. Mixtures with high relative proportions of phycocyanin have a strongly muted chlorophyll-*a* peak at 440 nm, and a shifted and partially muted peak chlorophyll-*a* peak at 660 nm.

abundance increases. This effect can be seen most clearly in the derivative spectra (Figure 11(*b*)). Note that the chlorophyll-*a* peak near 450 nm is muted in the mixtures of chlorophyll-*a* and phycocyanin due to masking from phycocyanin. The resulting derivative is asymmetric with a small peak at the blue end of the spectrum and a large peak at the red end of the spectrum. This pattern is evident in the derivative spectra for our filtered samples (Figure 3(*b*)). In the broad region where phycocyanin absorbs in the yellow-green portion of the spectrum around 620−630 nm, it interferes with the chlorophyll-*a* absorption peak at 680 nm, diminishing and shifting the position of the chlorophyll-*a* absorption peak towards longer wavelengths as the relative proportion of phycocyanin increases (Figure 11).

The Simis, Peters, and Gons (2005) algorithm corrects for biogenic backscatter and the interaction of phycocyanin with the chlorophyll-*a* absorption peak. Our results indicate that the algorithm of Simis, Peters, and Gons (2005) provided a better measure of chlorophyll-*a* in the most severely Case II waters that we studied, those with a high ratio of suspended sediment to phycocyanin. It is also worth noting that the Simis, Peters, and Gons (2005) algorithm was derived for cases where cyanobacteria were dominant, similar to the situation sometimes observed in the WB and SB. The satisfactory comparison of the Simis, Peters, and Gons (2005) and Witter et al. (2009) algorithms for low values of chlorophyll-*a* and low ratios of suspended sediment to phycocyanin suggests that the Simis semi-analytical approach may be more broadly applicable than was originally reported in Simis, Peters, and Gons (2005); however, this result should be verified with additional studies employing both remote sensing and field samples. Additional work with algorithms of this type or employing red : NIR ratios in Case II waters is warranted. The addition of correction factors for suspended sediment would likely be a fruitful direction for future algorithm development. This could be accomplished by ensuring that appropriate NIR bands are available on satellites or spectrometric

sensors used for chlorophyll-*a* estimation, because these bands are an important component of red : NIR-based empirical and semi-analytic algorithms.

5. Conclusions

The use of a lab-based, hyperspectral VNIR spectrometer with 210 bands enabled us to study the complete spectral response of the particulate load in the WB of Lake Erie and SB from 400 to 2500 nm. Our results enable us to quantify relative changes in phycocyanin and suspended sediment, which complicate the prediction of chlorophyll-*a* concentration in the WB and SB. The reflectance spectra can be decomposed by V-PCA into three pigment assemblages derived from the following: lake-dwelling blue-green algae in which chlorophyll-*a* and phycocyanin are both important CPAs; lake-dwelling diatoms and/or green algae in which chlorophyll-*a* is the dominant CPA; and a blue-green algal assemblage associated with goethite, a dissolved iron oxyhydroxide, in which chlorophyll-*a* and phycocyanin are also important CPAs. The spectral responses of these communities differ such that changes in their relative abundance alters the water-leaving radiance and complicates the retrieval of chlorophyll-*a*. In addition to complications arising from potential shifts in community structure, the reflectance spectra demonstrate significant influence due to the introduction of suspended sediment.

Despite these complications, our results indicate several points that are promising for the retrieval of plant pigment information from the WB of Lake Erie. Measures of CPAs collected from the surface of the water column were highly correlated with field-based estimates of k_T and published algorithms designed to correct for the bias of phycocyanin on chlorophyll-*a* performed well in both the WB and SB. Our approach should be applicable to other aquatic systems to differentiate the relative importance of various CPAs in Case II waters.

These results also indicate that the next generation of algorithms and instruments should monitor chlorophyll-*a*, and phycocyanin, and correct for the interference of phycocyanin on chlorophyll-*a* retrieval. The inclusion of NIR bands on future remote-sensing instruments to monitor suspended sediment is desirable since reliance on the 550 nm band for this purpose can be complicated by interference from phycocyanin and other biogenic factors.

Acknowledgements

We thank M. Thomas, Captain of the Stone Laboratory research vessels, Stone Laboratories, and Ohio Sea Grant for access and funds required to collect the samples (R/ER-078-ST) and develop the analytical methods (R/ES-010-ST; R/ER-088-PD; R/ER-100-PD). We also thank N. Tufillaro (COAS, Oregon State) for providing helpful comments regarding the article.

References

Alcântara, E., C. Barbosa, J. Stech, E. Novo, and Y. Shimbukuro. 2009. "Improving the Spectral Unmixing Algorithm to Map Water Turbidity Distributions." *Environmental Modelling and Software* 24: 1051–1061.

Amin, R., A. Gilerson, B. Gross, F. Moshary, and S. Ahmed. 2009. "MODIS and MERIS Detection of Dinoflagellates Blooms Using the RBD Technique." In *Proceedings of SPIE 7473, Remote Sensing of the Ocean, Sea Ice, and Large Water Regions*: 747304, September 9. http://dx.doi.org/10.1117/12.830631

Amin, R., J. Zhou, A. Gilerson, B. Gross, F. Monshary, and S. Ahmed. 2009. "Novel Optical Techniques for Detecting and Classifying Toxic Dinoflagellate Karenia Brevis Blooms Using Satellite Imagery." *Optics Express* 17: 9126–9144.

Armengol, J., L. Caputo, M. Comerma, C. Feijoó, J. C. García, R. Marcé, E. Navarro, and J. Ordoñez. 2003. "Sau Reservoir's Light Climate: Relationships Between Secchi Depth and Light Extinction Coefficient." *Limnetica* 22: 195–210.

Baban, S. M. J. 1995. "The Use of Landsat Imagery to Map Fluvial Sediment Discharge into Coastal Waters." *Marine Geology* 123: 263–270.

Balsam, W. L., and B. C. Deaton. 1991. "Sediment Dispersal in the Atlantic Ocean: Evaluation by Visible Light Spectra." *Review of Aquatic Sciences* 4: 411–447.

Barille, L., V. Meleder, J. P. Combe, P. Launeau, Y. Rince, V. Carrere, and M. Morancais. 2007. "Comparative Analysis of Field and Laboratory Spectral Reflectance of Benthic Diatoms with a Modified Gaussian Model Approach." *Journal of Experimental Marine Biology and Ecology* 343: 197–209.

Becker, B., D. Lusch, and J. Qi. 2005. "Identifying Optimal Spectral Bands from in situ Measurements of Great Lakes Coastal Wetlands Using Second-Derivative Analysis." *Remote Sensing of Environment* 97: 238–248.

Becker, R., M. I. Sultan, G. L. Boyer, M. R. Twiss, and E. Konopko. 2009. "Mapping Cyanobacterial Blooms in the Great Lakes Using MODIS." *Journal of Great Lakes Research* 35: 447–453.

Broersen, A., R. van Liere, and R. M. A. Heeren. 2005. "Comparing Three PCA-Based Methods for the 3D Visualization of Imaging Spectroscopy Data." In *Visualization, Imaging, and Image Processing*. Spain: Benidorm.

Buiteveld, H., J. M. H. Hakvoort, and M. Donze. 1994. "The Optical Properties of Pure Water." *SPIE Proceedings on Ocean Optics* 2258: 174–183.

Bukata, R. P., J. E. Bruton, and J. H. Jerome. 1983. "Use of Chromaticity in Remote Measurements of Water Quality." *Remote Sensing of Environment* 13: 161–177.

Clark, R. N., G. A. Swayze, R. Wise, K. E. Livo, T. M. Hoefen, R. F. Kokaly, and S. J. Sutley. 2003. "USGS Digital Spectral Library splib05a." *USGS Open File Report* 03-395, Denver CO: US Geologic Survey. http://pubs.usgs.gov/of/2003/ofr-03-395/ofr-03-395.html

Combe, J. P., P. Launeau, V. Carrere, D. Despan, V. Meleder, L. Barille, and C. Sotin. 2005. "Mapping Microphytobenthos Biomass by Non-Linear Inversion of Visible-Infrared Hyperspectral Images." *Remote Sensing of Environment* 98: 371–387.

Dabakk, E., M. Nilsson, P. Geladi, S. Wold, and I. Renberg. 1999. "Inferring Lake Water Chemistry from Filtered Seston Using NIR Spectrometry." *Water Research* 34: 1666–1672.

Deaton, B. C., and W. L. Balsam. 1991. "Visible Spectroscopy: A Rapid Method for Determining Hematite and Goethite Concentrations in Geological Materials." *Journal of Sedimentary Petrology* 61: 628–632.

DeCauwer, V., K. Ruddick, Y. J. Park, B. Nechad, and M. Kryamarios. 2004. "Optical Remote Sensing in Support of Eutrophication Monitoring in the Southern North Sea." *EARSel eProceedings* 3: 208–221.

de Medeiros, V., A. M. Ugulino, R. Kawakami, H. Galvao, C. da Silva, S. T. Bezerra, T. I. Salata, M. do Scorro, R. de Oliveira, F. A. Barbosa, and N. M. Mariano. 2005. "Screening Analysis of River Seston Downstream of an Effluent Discharge Point Using Near-Infrared Reflectance Spectrometry and Wavelet-Based Spectral Region Selection." *Water Research* 39: 3089–3097.

Demetriades-Shah, T., M. Stevens, and J. Clark. 1990. "High Resolution Derivative Spectra in Remote Sensing." *Remote Sensing of Environment* 33: 55–64.

Frouin, R., P. Y. Deschamps, L. Gross-Colzy, H. Murakami, and T. Y. Nakajima. 2006. "Retrieval of Chlorophyll-a Concentration via Linear Combination of Global Imager Data." *Journal of Oceanography* 62: 331–337.

Frouin, R., P. Y. Deschamps, J. M. Nicolas, and P. Dubuisson. 2005. "Ocean Color Remote Sensing through Clouds." In *Proceedings of SPIE 5885, Remote Sensing of the Coastal Oceanic Environment*: 588504, September 10. http://dx.doi.org/10.1117/12.621055.

Gilerson, A., A. Gitelson, J. Zhou, I. Ioannou, and S. Ahmed. 2009. "Remote Estimation of Chlorophyll-a in Coastal Waters Using Red and Near Infra-red Spectral Regions." In *Proceedings of V International Conference*, Vol. 8–11, "Current Problems in Optics of Natural Waters (ONW)", St Petersburg, 110–114. Moscow: Russian Academy of Sciences.

Gitelson, A. 1992. "The Peak near 700nm on Reflectance Spectra of Algae and Water: Relationships of its Magnitude and Position with Chlorophyll Concentration." *International Journal of Remote Sensing* 13: 3367–3373.

Gitelson, A., G. Dall'Olmo, W. Moses, D. Rundquest, T. Barrow, T. Fisher, D. Gurlin, and J. Holz. 2008. "A Simple Semi-Analytical Model for Remote Sensing Estimation of Chlorophyll-a in Turbid Waters: Validation." *Remote Sensing of Environment* 112: 3582–3593.

Gitelson, A., G. Keydan, and V. Shiskin. 1985. "Inland Water Quality Assessment from Satellite Data in Visible Range of the Spectrum." *Soviet Remote Sensing* 6: 28–36.

Gons, H. J. 1999. "Optical Teledetection of Chl a in Turbid Inland Waters." *Environmental Science Technology* 33: 1127–1132.

Grahm, J. 1966. "Secchi Disk Observations and Extinction Coefficients in the Central and Eastern North Pacific Ocean." *Limnology and Oceanography* 11: 184–190.

Gross-Colzy, L., S. Colzy, R. Frouin, and P. Henry. 2007. "A General Ocean Colour Atmospheric Correction Scheme Based on Principal Component Analysis – Part I: Performance on Case I and Case 2 Waters." In *Proceedings of SPIE 6680, Coastal Ocean Remote Sensing*: 668002, September 28. http://dx.doi.org/10.1117/12.738508

Han, L., and D. Rundquist. 1997. "Comparison of NIR/Red Ratio and First Derivative of Reflectance in Estimating Algal-Chlorophyll Concentration: A Case Study in a Turbid Reservoir." *Remote Sensing of Environment* 62: 253–261.

Harris, S. E., and A. C. Mix. 1999. "Pleistocene Precipitation Balance in the Amazon Basin Recorded in Deep-Sea Sediments." *Quaternary Research* 51: 14–26.

Islam, M. R., Y. Yamaguchi, and K. Ogawa. 2001. "Suspended Sediment in the Ganges and Brahmaputra, Rivers in Bangladesh: Observation from TM and AVHRR Data." *Hydrological Processes* 15: 493–509.

Jarrard, R. D., and M. D. Vanden Berg. 2006. "Sediment Mineralogy Based on Visible and Near-Infrared Reflectance Spectroscopy." In *New Techniques in Sediment Core Analysis*, Vol. 267, a edited by R. G. Rothwell, 129–140. London: Geological Society of London Special Publications.

Kachigan, S. K. 1991. *Multivariate Statistical Analysis: A Conceptual Introduction*. New York: Radius Press.

Kaiser, H. F. 1958. "The Varimax Criteria for Analytic Rotation in Factor Analysis." *Psychometrica* 23: 187–200.

Kelble, C. R., P. B. Ortner, G. L. Hitchcock, and J. N. Boyer. 2005. "Attenuation of Photosynthetically Available Radiation (PAR) in Florida Bay: Potential for Light Limitation of Primary Producers." *Estuaries* 28: 560–571.

Lahet, F., S. Ouillon, and P. Forget. 2000. "A Three-Component Model of Ocean Colour and Its Application in the Ebro River Mouth Area." *Remote Sensing of Environment* 72: 181–190.

Le, C., Y. Li, Y. Zha, D. Sun, C. Huang, and H. Lu. 2009. "A Four-Band Semi-Analytic Model for Estimating Chlorophyll a in Highly Turbid Lakes: The Case of Taihu Lake, China." *Remote Sensing of Environment* 113: 1175–1182.

Lorenzen, M. W. 1980. "Use of Chlorophyll-Secchi Disk Relationships." *Limnology and Oceanography* 25: 371–372.

Martin, S. 2004. *An Introduction to Ocean Remote Sensing*. Cambridge: Cambridge University Press.

McClain, C. R. 2009. "A Decade of Satellite Ocean Color Observations." *Annual Review of Marine Science* 1: 19–42.

Méléder, V., L. Barille, P. Launeau, V. Carrere, and Y. Rince. 2003. "Spectrometric Constraint in Analysis of Benthic Diatom Biomass Using Monospecific Cultures." *Remote Sensing of Environment* 88: 386–400.

Millie, D. F., G. L. Fahnenstiel, J. Dyble Bressie, R. J. Pigg, R. R. Rediske, D. M. Klarer, P. A. Tester, and R. W. Littaker. 2009. "Late-Summer Phytoplankton in Western Lake Erie (Laurentian Great Lakes): Bloom Distributions, Toxicity, and Environmental Influences." *Aquatic Ecology* 43: 915–934. doi:10.1007/s10452-009-9238-7.

Mix, A. C., S. E. Harris, and T. R. Janecek. 1995. "Estimating Lithology from Nonintrusive Reflectance Spectra: Leg 138." In *Proceedings of ODP Scienctific Results*, Vol. 138, edited by N. G. Pisias, L. A. Mayer, T. R. Janecek, A. Palmer-Julson, and T. H. van Andel, 413–427. College Station, TX: Ocean Drilling Program.

Mix, A. C., D. C. Lund, N. G. Pisias, P. Boden, L. Bornmalm, M. Lyle, and J. Pike. 1999. "Rapid Climate Oscillations in the Northeast Pacific During the Last Deglaciation Reflect Northern and Southern Hemisphere Sources." In *Mechanisms of Global Climate Change at Millennial Time Scales, Geophysical Monograph Series*, Vol. 112, edited by P. U. Clark, S. Webb and D. Keigwin, 127–148. Washington, DC: AGU.

Moberg, L., B. Karlberg, K. Sørensen, and T. Kallqvist. 2002. "Assessment of Phytoplankton Class Abundance Using Absorption Spectra and Chemometrics." *Journal of Talanta* 56: 153–160.

Mobley, C. D., D. Stramski, W. P. Bissett, and E. Boss. 2004. "Optical Modelling of Ocean Waters: Is the Case 1–Case 2 Classification Still Useful?" *Journal of Oceanography* 17: 60–67.

Montero Sanchez, I. C., and G. H. Brimhall. 2001. "Semi-automated Mineral Identification Algorithm for Ultraviolet, Visible, and Near-Infrared Reflectance Spectroscopy." In *International Association of Mathematical Geology Proceedings 6th Annual Conference of the International Association for Mathematical Geology IAMG*, Cancun, September 6–12.

Morel, A., and L. Prieur. 1977. "Analysis of Variations in Ocean Color." *Limnology and Oceanography* 22: 709–722.

Murphy, R., A. Underwood, T. Tolhurst, and M. Chapman. 2008. "Field-Based Remote-Sensing for Experimental Intertidal Ecology: Case Studies Using Hyperspatial and Hyperspectral Data from New South Wales (Australia)." *Remote Sensing of Environment* 112: 3353–3365.

Nellis, M. D., J. A. Harrington Jr., and J. Wu. 1998. "Remote Sensing of Temporal and Spatial Variations in Pool Size, Suspended Sediment, Turbidity, and Secchi Depth in Tuttle Creek Reservoir, Kansas: 1993." *Geomorphology* 21: 281–293.

Ortiz, J. D., S. O'Connell, J. DelViscio, W. Dean, J. Carriquiry, T. Marchitto, Y. Zheng, and A. van Geen. 2004. "Enhanced Marine Productivity off Western North America During Warm Climate Intervals of the Past 52 Kyr." *Geology* 32: 521–524.

Ortiz, J. D., S. O'Connell, and A. Mix. 1999. "Data Report: Spectral Reflectance Observations from Leg 162 Recovered Sediments." In *Proceedings of ODP, Scientific Results*, Vol. 162, 259–264. College Station, TX: Ocean Drilling Program.

Ortiz, J. D., L. Polyak, J. M. Grebmeier, D. A. Darby, D. D. Eberl, and S. Naidu. 2009. "Provenance of Holocene Sediment on the Chukchi-Alaskan Margin Based on Combined Diffuse Spectral Reflectance and Quantitative X-Ray Diffraction Analysis." *Global and Planetary Change* 68: 73–84.

Ouellette, A. J., S. M. Handy, and S. W. Wilhelm. 2006. "Toxic Microcystis Is Widespread in Lake Erie: PCR Detection of Toxin Genes and Molecular Characterization of Associated Cyanobacterial Communities." *Microbial Ecology* 51: 154–165.

Ouillon, S., P. Douillet, and S. Andrefouet. 2004. "Coupling Satellite Data with *in situ* Measurement and Numerical Modeling to Study Fine Suspended-Sediment Transport: A Study for the Lagoon of New Caledonia." *Coral Reefs* 23: 109–122.

Ouillon, S., P. Forget, F. Lahet, and Y. Lucas. 1997. "Optical Properties of Sediment-Loading Marine Waters: First Results on the Influence of Goethite." In *Proceedings of the 4th International Conference on Remote Sensing for Marine and Coastal Environments*, ERIM, Vol. 2, 13–22, Orlando, FL, March 17–19.

Park, Y.-J., K. Ruddick, and G. Lacroix. 2010. "Detection of Algal Blooms in European Waters Based on Satellite Chlorophyll Data from MERIS and MODIS." *International Journal of Remote Sensing* 31: 6567–6583.

Peng, F., S. Effler, D. O'Donnell, M. Perkins, and A. Weidemann. 2007. "Role of Minerogenic Particles in Light Scattering in Lakes and a River in Central New York." *Applied Optics* 46: 6577–6594.

Randolph, K., J. Wilson, L. Tedesco, L. Li, D. Lani Pascual, and E. Soyeux. 2008. "Hyperspectral Remote Sensing of Cyanobacteria in Turbid Productive Water Using Optically Active Pigments, Chlorophyll a and Phycocyanin." *Remote Sensing of Environment* 112: 409–4019.

Robertson, P., L. A. Lawton, and B. Cornish. 1999. "The Involvement of Phycocyanin Pigment in the Photodecomposition of the Cyanobacterial Toxin, Microcystin-LR." *Journal of Porphyrins and Phthalocyanines* 3: 544–551.

Roesler, C. S., and E. Boss. 2008. "In Situ Measurement of the Inherent Optical Properties (IOPs) and Potential for Harmful Algal Bloom (HAB) Detection and Coastal Ecosystem Observations." In *Real-Time Coastal Observing Systems for Marine Ecosystem Dynamics and Harmful Algal*

Blooms: Theory, Instrumentation and Modelling, edited by M. Babin,C. S. Roesler, and J. Cullen, 153–206. Paris: UNESCO.

Schalles, J. F. 2006. "Optical Remote Sensing Techniques to Estimate Phytoplankton Chlorophyll *a* Concentrations in Coastal Waters with Varying Suspended Matter and CDOM Concentrations." In *Remote Sensing of Aquatic Coastal Ecosystem Processes: Science and Management Applications*, edited by L. Richardson and E. Ledrew, 27–79 Dordrecht: Springer.

Schalles, J. F., and Y. Z. Yacobi. 2000. "Remote Detection and Seasonal Patterns of Phycocyanin, Carotenoid, and Chlorophyll Pigments in Eutrophic Waters." *Advancements in Limnology* 55: 153–168.

Schlens, J. 2005. "A Tutorial on Principal Component Analysis." Accessed June 1, 2010. http://www.snl.salk.edu/~shlens/pca.pdf

Shuchman, R., A. Korosov, C. Hatt, D. Pozdnyakov, J. Means, and G. Meadows. 2006. "Verification and Application of a Bio-Optical Algorithm for Lake Michigan Using SeaWIFS: A 7 Year Inter-Annual Analysis." *Journal of Great Lakes Research* 32: 258–279.

Simis, S. G. H., S. W. M. Peters, and H. J. Gons. 2005. "Remote Sensing of the Cyanobacterial Pigment Phycocyanin in Turbid Inland Water." *Limnology and Oceanography* 50: 237–245.

Smith, L. I. 2002. "A Tutorial on Principal Components Analysis." Accessed June 1, 2010. http://kybele.psych.cornell.edu/edelman/Psych-465-Spring-2003/PCA-tutorial.pdf

Steinmetz, F., P. Y. Deschamps, and D. Ramon. 2008. "Atmospheric Correction in Presence of Sun Glint: Application to MERIS." In *Second MERIS (A)ATSR Workshop*, 22–26, ESRIN, Franscati, September 22–26.

Sze, P. 1986. *A Biology of the Algae*. Dubuque, IA: Wm. C. Brown. ISBN 0-697-00741-3.

Tarrant, P., and S. Neuer. 2009. "Monitoring Algal Blooms in a Southwestern U.S. Reservoir System." *EOS* 90: 38–39.

Toepel, J., U. Langner, and C. Wilhelm. 2005. "The Combination of Flow Cytometry and Single Cell Absorption Spectroscopy to Study the Phytoplankton Structure and to Calculate the Chl a Specific Absorption Coefficients at the Taxon Level." *Journal of Phycology* 41: 1099–1109.

Tyler, A. N., E. Svab, T. Preston, M. Présing, and W. A. Kovács. 2006. "Remote Sensing of the Water Quality of Shallow Lakes: A Mixture Modelling Approach to Quantifying Phytoplankton in Water Characterized by High-Suspended Sediment." *International Journal of Remote Sensing* 27: 1521–1537.

Tyler, J. E. 1968. "The Secchi Disk." *Limnology and Oceanography* 13: 1–6.

USGS. "Stream flow Database." Accessed June 1, 2010. http://waterdata.usgs.gov/nwis/dv/referred_module=sw

Viscara Rossel, R. A., R. N. McGlynn, and A. B. McBratney. 2006. "Determining the Composition of Mineral-Organic Mixes Using UV-VIS-NIR Diffuse Reflectance Spectroscopy." *Geoderma* 137: 70–82.

Wass, P. D., S. D. Marks, J. W. Finch, G. J. L. Leeks, and J. K. Ingram. 1997. "Monitoring and Preliminary Interpretation of in-River Turbidity and Remote Sensed Imagery for Suspended Sediment Transport Studies in the Humber Catchment." *The Science of the Total Environment* 194/195: 263–283.

Will, G. 2006. *Powder Diffraction the Rietveld Method and the Two-Stage Method*. Berlin: Springer.

Witter, D. L., J. D. Ortiz, S. Palm, R. T. Heath, and J. W. Budd. 2009. "Assessing the Application of SeaWiFS Ocean Color Algorithms to Lake Erie." *Journal of Great Lakes Research* 35: 361–370.

Wolfe, A. P., R. D. Vinebrooke, N. Michelutti, B. Rivard, and B. Das. 2006. "Experimental Calibration of Lake-Sediment Spectral Reflectance to Chlorophyll a Concentrations: Methodology and Paleolimnological Validation." *Journal of Paleolimnology* 36: 91–100.

Woźniak, S. B., and D. Stramski. 2004. "Modeling the Optical Properties of Mineral Particles Suspended in Seawater and Their Influence on Ocean Reflectance and Chlorophyll Estimation from Remote Sensing Algorithms." *Applied Optics* 43: 3489–3503.

Wynne, T. T., R. P. Stumpf, M. C. Tomlinson, and J. Dyble. 2010. "Characterizing a Cyanobacterial Bloom in Western Lake Erie Using Satellite Imagery and Meteorological Data." *Limnology and Oceanography* 55: 2025–2036.

Yew-Hoong Gin, K., S. Teck Koh, I. I. Lin, and E. Soon Chan. 2002. "Application of Spectral Signatures and Colour Ratios to Estimate Chlorophyll in Singapore's Coastal Waters." *Estuarine Coastal and Shelf Science* 55: 719–728.